Final-state distributions in resonant charge transfer by ions on Rydberg atoms

D. S. Fisher, C. W. Fehrenbach, and S. R. Lundeen
Department of Physics, Colorado State University, Ft. Collins, Colorado 80523

E. A. Hessels
Department of Physics, York University, Toronto, Ontario, Canada M3J 1P3

B. D. DePaola
Department of Physics, Kansas State University, Manhattan, Kansas 66506
(Received 29 April 1997)

Charge-transfer collisions between He^+ ions at $v=0.1$ a.u. and excited states of Rb with $n_t=7-14$ have been studied, using a laser-based method of analyzing the final-state distribution. A Doppler-tuned CO_2 laser is used to selectively detect one particular final state (n,L) and directly measure the fraction of the total charge transfer product contained in that one level. The fractional population shows clear resonant behavior as a function of target excitation level (n_t). Measurements were made for $n=10$ levels of helium with $L=4$, 5, and 7–9, and for the $9G$ level. The results are compared with predictions of classical trajectory Monte Carlo calculations. [S1050-2947(97)00712-9]

PACS number(s): 34.70.+e, 34.60.+z

INTRODUCTION

Charge-transfer collisions between an ion of charge Q and a highly excited atom with principal quantum number n occur with quite large cross section, approximately $Qn^4a_0^2$ for sufficiently low ion velocity. Such collisions result in a narrow distribution of final states with the captured electron being bound by approximately the same energy as in the original excited atom, and for this reason are referred to as ''resonant'' charge-transfer collisions. No satisfactory quantum-mechanical calculation of the process exists, and all practical theoretical predictions to date are obtained from classical models. The most successful of these, the classical trajectory Monte Carlo model (or CTMC) uses repeated integration of the classical equations of motion, assuming initial classical orbits chosen randomly from a statistical distribution that mimics the quantum-mechanical state. The quantum numbers for the final state are assigned based on the final classical orbits found after charge capture [1]. The resonant nature of the capture is physically plausible at very low collision velocities, where the electron would be expected to evolve adiabatically in the double potential well of the two slowly moving ions. The actual classical calculations carried out to date have been at velocities comparable or larger than the ''matching velocity,'' where the projectile velocity is equal to the orbital velocity of the target electron, $v_n=\alpha c/n$. These calculations show a finite distribution of final energies which broadens as the projectile velocity increases. Since the CTMC approach is not expected to be valid at very low velocities, it is still not clear just how ''resonant'' such collisions could become at velocities well below the matching velocity.

In this study, we examine the final-state distribution in ion–Rydberg-atom charge transfer by measuring the fraction of the total population found in a particular n,L level. This is a much more specific diagnostic of the population distribution than has been obtained to date with other methods. The measured value of this population fraction is observed to vary smoothly with the excitation energy of the Rydberg target. Both the absolute values of these fractional populations and their variation with target excitation energy pose very quantitative tests for theories of the resonant charge transfer process.

PREVIOUS EXPERIMENTAL STUDIES

Experimental studies of ion–Rydberg-atom resonant charge-transfer collisions were pioneered by MacAdam and co-workers [2]. In a series of experiments, a beam of ions crossed a thermal alkali beam excited to Rydberg levels by pulsed lasers, and the final state of the charge-transfer product was analyzed by Stark ionization. In this method, the principal quantum number of the final state is inferred by measuring the electric field at which the atom ionizes. The experimental data are ion flux versus ionizing field, and this is mapped into an n distribution by assuming that ionization occurs at the classical ionization field:

$$E_{S.I.}(n)=\frac{1}{16n^4}\ \text{a.u.} \tag{1}$$

n distributions derived in this way were obtained by MacAdam in studies of collisions by Na^+ on $Na(nS$ or $nD)$ for a few n's in the range 24–34 and a ion velocity range of approximately 0.9–1.7 times the matching velocity [2]. The results generally confirm the resonant nature of the capture, but differ in detail from the predictions of CTMC calculations. Whether this indicates a deficiency in the CTMC predictions, or the difficulty in extracting an unambiguous n distribution from such Stark ionization data is not yet clear. The problem is that the actual route to Stark ionization can be much more complicated than a simple one-to-one correspondence suggested by Eq. (1); the actual ionization field for levels sharing the same principal quantum number can

 © 1997 The American Physical Society

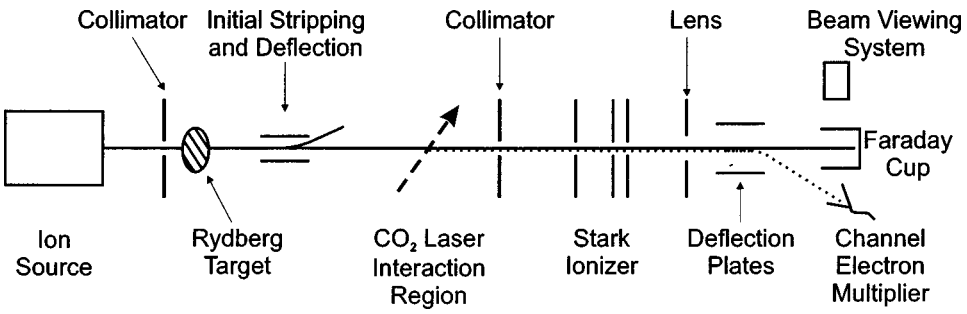

FIG. 1. Schematic diagram of the experimental apparatus. A 1-keV He^+ beam is extracted from a Colutron ion source, tighly collimated, and sent through a Rb (nF) Rydberg target where about 1% of the ions capture electrons to form Rydberg helium levels. A short electric field region after the target deflects remaining ions and ionizes highly excited levels. The atomic beam then intersects a CO_2 laser beam, at a variable angle, Doppler tuning the laser to excite various 10-30 or 9-20 transitions in helium. The laser excited atoms are subsequently Stark ionized and the resulting ions collected in a Channeltron electron multiplier. A beam viewer, located opposite to the Channeltron, is optionally used while adjusting the focusing lens in the detector. The neutral atomic beam is monitored by the secondary electron emission from a Faraday cup on axis.

vary by as much as a factor of three [3]. The Stark ionization technique can only infer the n distribution by making assumptions regarding the L and m distributions, for example, that only $m=0$ states are populated. Since neither the L nor the m distributions can be determined from the Stark ionization data, this precludes a precise test of theoretical predictions.

Recently, a similar method was applied to study charge capture collisions by multiply charged ions on Rydberg atoms [4,5]. A thermal Rb beam, excited by a single UV laser to the $17P$ state was crossed with a Kr^{8+} beam and the product Kr^{7+} beam was analyzed with a Stark ionization detector. The experimental results show rather broad n distributions, but substantially narrower than the CTMC predictions. As in the studies with singly charged ions, the lack of any resolution of L or m states, coupled with the inherent ambiguity involved in inferring n from the Stark ionization field all cloud the interpretation of the experimental results, which at face value seem to show clear deviations from the predictions of CTMC.

RESIS METHOD FOR STUDYING CHARGE TRANSFER COLLISIONS

In this study, a laser is used to spectroscopically resolve a single charge-transfer product level whose population is to be measured. Stark ionization plays a role in the detection process, but it is not the selective element. A Doppler-tuned CO_2 laser excites the chosen level (a particular $n=9$ or $n=10$ level) to a very highly excited discrete level, which is then Stark ionized. The resulting ions are efficiently collected, and since only atoms in the chosen level can be excited and ionized, the ion current is a measure of the population in the selected level. This method is sometimes called RESIS, for resonant excitation Stark ionization spectroscopy. It was applied to study the L distributions obtained in charge transfer by slow S^+ ions incident on $8F$ and $10F$ levels of Rb [6] and demonstrated clearly that the L distributions were nonstatistical.

Here, we apply the same technique to study charge transfer between He^+ ions and excited Rb atoms. The primary focus of this study is on the n distribution of the charge capture products, which reflects the energy-resonant capture. Unfortunately, it is not yet possible to directly measure the population distribution in a wide range of n states with the RESIS technique since only $n=9$ and 10 levels can be detected with the CO_2 laser. However, it is still possible to study the resonant nature of the charge transfer collision by measuring the fractional population in a fixed level, such as the $10G$ level, as a function of the excitation level (n_t) of the Rydberg target. Such a measurement gives a similar test of calculations, and can be conveniently obtained with the RESIS method. It can also be carried out with several specific L levels, allowing their populations to be compared. We describe below measurements of this type for $10G$, $10H$, and 10 high-L ($L=7,8,9$) levels for $7\leqslant n_t\leqslant 14$, and the $9G$ level for $7\leqslant n_t\leqslant 10$.

EXPERIMENTAL TECHNIQUE

The experimental apparatus is shown schematically in Fig. 1. A beam of He^+ ions of 1.00-keV energy is obtained from a Colutron ion source and, after analysis in an $E\times B$ velocity filter, is transmitted through a small aperture (2 mm diameter) into the Rydberg target region. The Rydberg target is a dense thermal Rb beam excited by three cw lasers to the nF level, where $7\leqslant n_t\leqslant 14$ [7,8]. The first laser, a diode laser at 780 nm, excites the $5S_{1/2}(F=2)$-$5P_{3/2}(F=3)$ transition in ^{87}Rb. The second laser, a NaCl color center laser at 1529 nm, further excites the atoms to the $4D_{5/2}(F=4)$ level. The final laser, a Ti:sapphire laser, can be tuned to excite any one of the $nF_{7/2}(F=5)$ levels for $7\leqslant n_t\leqslant 14$. The density of nF atoms produced is sufficient in all cases to produce large gain on the transition from the nF state to the $(n+1)D$ level, which lies just below it, resulting in rapid sharing of the excited population between these two levels, as was described in detail previously for the $10F$ target [8]. We estimate the total excited-state population in the Rydberg target as about 2×10^8 excited atoms in a spherical volume of about 3.6 mm diameter, giving a target thickness of about 10^9 cm^{-2}. This is sufficient to neutralize about 1% of the He^+ beam for the $10F$ target.

After the Rydberg target, the atoms pass through a short ($t=0.1$ μs) electric field region, which may be used to deflect the residual He^+ ions from the beam ($E=20$ V/cm) or

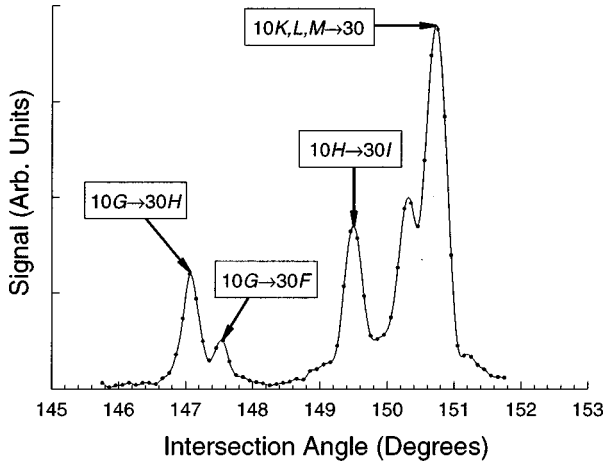

FIG. 2. RESIS excitation spectrum of 10-30 transitions in helium, showing the resonance lines used for detection of 10*G*, 10*H*, and 10 high-*L* populations after resonant charge capture in the Rydberg target. The laser frequency is 975.930 cm^{-1}.

(optionally) to Stark ionize very highly excited levels ($E = 3300$ V/cm). Then, after a total drift time of 1.9 μs, they intersect the beam of a cw CO_2 laser. This laser is operated in a single transverse and longitudinal mode on the 10R20 line at a frequency of 975.930 cm^{-1} with a total power of about 6 W. The laser beam is Gaussian in shape with a waist size of about 1.6 mm located 7 m prior to the interaction point with the fast beam.

Fine control of this laser's frequency in the atom's rest frame is obtained through the Doppler effect, by varying the angle of intersection between the laser and the fast He beam. When the angle of intersection is approximately 150° from antiparallel, the Doppler-tuned frequency is correct for exciting the 10-30 transition in helium. The $n=30$ atoms are Stark ionized and the resulting ions collected. Figure 2 shows the dependence of the observed ion current on the Doppler-tuning angle in the CO_2 laser region. The large peak is due to the unresolved excitation of 10 *K*, *L*, and *M* states to $n=30$. The excitation of the 10*I* state is partially resolved on the shoulder of this peak. The 10*H* and 10*G* excitations are fully resolved. The main feature in the 10*G* excitation resonance is due to the 10*G*-30*H* excitation. The weaker feature is the 10*G*-30*F* excitation, which occurs about 90 MHz lower in frequency. When the CO_2 laser is tuned to the 10*G* peak, the ion current is entirely due to excitation of atoms in this level and is therefore a direct measure of the population of the 10*G* level. Similar signals can be obtained that measure the 10*H* population, or the sum of 10*K*,*L*,*M* populations, by simply tuning the CO_2 laser to the corresponding positions in the spectrum of Fig. 2. The CO_2 laser can also be used to excite $n=9$ levels to $n=20$, giving probes of the populations of several $n=9$ levels.

The Rydberg state detector which follows the CO_2 laser excitation is preceded by a 2 mm×2 mm square collimator. Together with the pre-Rydberg target 2-mm collimator, this restricts the beam to an angular width of 2 mrad full width at half maximum (FWHM). The Rydberg detector is a sequence of planar electrodes, arranged to produce a long region of slowly increasing potential followed by a shorter region in which the potential falls rapidly. The length of the long region is three times that of the short region, so that the field in the long region is one-third of the ionizing field, E_0, in the short region. The applied potential is adjusted so that all atoms of the desired principal quantum number, e.g., $n=30$, will ionize completely in the field E_0, but none of them will ionize in the field $E_0/3$ present in the long region. This means that atoms in the desired state all ionize at the high potential, and the resulting ions are accelerated as they return to ground potential. This boost in energy tags the signal ions so that they can be distinguished from background ions present in the beam because of collisional ionization in background gas collisions.

The Rydberg detector is designed to produce efficient ionization and collection of atoms in a particular *n* level, in contrast with other detectors that are designed to distinguish populations of different *n* levels. All indications are that it achieves this objective. For example, when used to detect $n=30$ atoms, the signal current begins to rise when a field of 550 V/cm is applied in the short region, and continues to rise over a factor of 2 in field, after which it is approximately constant until a field of 1650 V/cm is applied. At this and higher fields, $n=30$ atoms are beginning to ionize in the long region, producing ions that are not energy tagged and are therefore not detected as signal. Over a considerable range of ionizing field, it appears that 100% of the $n=30$ atoms are being ionized and tagged.

Following the ionizer, a single Einzel lens is used to focus the RESIS signal ions onto a detector. The focused spot is about 3 mm in diameter. The detector is a Channeltron electron multiplier with an entrance aperture of 6 mm, allowing for 100% collection of the signal ions. The channeltron is located 7.5 cm below the atomic beam axis, and the ions are steered into it by a set of *XY* deflector plates. Alternatively, the *Y* deflection voltage can be reversed and the signal ions deflected upwards into a Beam Viewer (Colutron BVS-1), located opposite the Channeltron, which allows the Einzel lens to be adjusted for best beam definition.

The CO_2 laser used in the RESIS excitation is modulated by an optical chopper, and the Channeltron current synchronous with this chopping is detected by a lock-in amplifier. At the same time as the population of a particular level is probed with the RESIS signal, we also wish to determine the intensity of the total neutral beam produced in the Rydberg target. This is accomplished with an unsuppressed Faraday cup detector, placed on the beam axis downstream of the Stark ionizer and deflection plates. Since the neutral beam passes through the detector without deflection, it will hit the Faraday cup and cause a secondary emission current. To determine the portion of the neutral beam, which is due to neutralization in the Rydberg target (as opposed to neutralization from collisions with background gas), we modulate one of the Rydberg target excitation lasers ($\lambda=1.529$ nm) with a second optical chopper, and detect the synchronous portion of the secondary emission current with a second lock-in amplifier. The two chopping frequencies are sufficiently different (199 Hz for the Rydberg target, 277 Hz for the CO_2 laser) that both lock-in signals can be measured simultaneously. A third lock-in amplifier monitors the strength of the Rydberg target by measuring the blue light $[(n+1)D\text{-}5P]$ emitted by the target synchronous with the

TABLE I. Determination of fractional population of helium nL levels after electron capture by He^+ at $v=0.1$ a.u. from several Rydberg targets. Column one indicates the target excitation. Column 2 gives the measured ratio between the peak nL RESIS signal and the neutral beam signal. Column 3 lists the number of independent measurements of this ratio. Column 4 gives the fractional nL population at the CO_2 laser, with the common 20% error due to the uncertainty in the excitation efficiency not shown. Column 5 shows the correction factor to naive spontaneous decay deduced from simulations of cascades and blackbody-induced transitions in the 1.9 μs between target and CO_2 laser, column 6 shows the fractional population at the time of capture, again not showing the common systematic error. Column 7 shows the predicted population fraction at capture, using CTMC.

			10G			
Target	$S(10G)/I$	No. reps.	$f(10G)_{\text{laser}}$	F_{10G}	$f(10G)_0$	Theory
7F/8D	1.305(25)	12	0.285(5)%	1.07	0.759(15)%	1.72(7)%
8F/9D	1.646(31)	12	0.359(7)%	1.11	0.921(18)%	2.36(8)%
9F/10D	1.213(11)	12	0.264(3)%	1.15	0.655(6)%	1.72(6)%
10F/11D	0.945(18)	14	0.206(4)%	1.18	0.498(10)%	1.33(5)%
11F/12D	0.830(16)	12	0.181(3)%	1.23	0.420(8)%	1.02(4)%
12F/13D	0.696(13)	12	0.152(3)%	1.27	0.341(7)%	0.82(4)%
13F/14D	0.664(13)	12	0.145(3)%	1.31	0.315(6)%	0.79(5)%
14F/15D	0.542(10)	8	0.118(2)%	1.34	0.252(4)%	0.64(5)%
			9G			
Target	$S(9G)/I$	No. reps.	$f(9G)_{\text{laser}}$	F_{9G}	$f(9G)_0$	Theory
7F/8D	0.473(18)	3	0.103(4)%	1.12	0.388(13)%	3.97(12)%
8F/9D	0.354(14)	3	0.077(3)%	1.32	0.247(9)%	2.29(8)%
9F/10D	0.298(11)	3	0.064(2)%	1.46	0.182(7)%	1.58(6)%
10F/11D	0.253(7)	6	0.055(2)%	1.68	0.138(4)%	1.19(5)%
			10H			
Target	$S(10H)/I$	No. reps.	$f(10H)_{\text{laser}}$	F_{10H}	$f(10H)_0$	Theory
7F/8D	1.678(42)	7	0.366(9)%	1.08	0.676(18)%	1.31(6)%
8F/9D	2.491(67)	6	0.543(14)%	1.12	0.968(26)%	2.74(9)%
9F/10D	1.973(53)	6	0.430(12)%	1.15	0.746(20)%	1.74(6)%
10F/11D	1.721(39)	8	0.375(8)%	1.18	0.635(14)%	1.38(5)%
11F/12D	1.611(41)	6	0.351(9)%	1.23	0.569(15)%	1.14(4)%
12F/13D	1.397(37)	6	0.305(8)%	1.26	0.483(13)%	0.78(4)%
13F/14D	1.393(37)	6	0.304(8)%	1.30	0.467(13)%	0.69(4)%
14F/15D	1.101(36)	4	0.240(8)%	1.34	0.357(11)%	0.72(5)%
			10 High-L ($L=7,8,\&9$)			
Target	$S(10\text{Hi-}L)/I$	No. reps.	$f(10\text{Hi-}L)_{las}$	$F_{10\text{Hi-}L}$	$f(10\text{Hi}L)_0$	Theory
7F/8D	2.82(7)	7	0.615(15)%	1.14	0.721(18)%	1.53(6)%
8F/9D	5.48(15)	6	1.194(31)%	1.17	1.363(35)%	3.06(9)%
9F/10D	6.39(17)	6	1.393(37)%	1.20	1.550(41)%	2.60(7)%
10F/11D	7.45(17)	8	1.625(37)%	1.23	1.765(40)%	2.12(6)%
11F/12D	7.09(19)	6	1.546(41)%	1.26	1.640(43)%	2.12(6)%
12F/13D	5.68(15)	6	1.239(33)%	1.29	1.283(33)%	1.82(5)%
13F/14D	5.59(15)	6	1.220(33)%	1.33	1.225(33)%	1.51(5)%
14F/15D	4.29(14)	4	0.935(30)%	1.36	0.918(29)%	1.50(6)%

chopping of the Rydberg target. The three lock-in signals are digitally averaged and recorded by a computer.

RESULTS AND CONCLUSIONS

To determine the strength of the 10G RESIS signal, measurements were made at six angles spanning the central portion of the excitation resonance. Each measured signal was normalized to the neutral beam signal measured simultaneously, and then the six signal-to-beam ratios were fit to a Gaussian line shape to extract the peak signal-to-beam ratio. This procedure was repeated several times on two to four separate days for all eight choices of target excitation, n_t. In this way, 8–14 independent measurements of the peak signal-to-beam ratio were made for each target. The average results for each target are shown in Table I. The scatter between repeated measurements was consistent with a statistical uncertainty of about 6% for each independent measure-

ment, and the final statistical errors in the average ratios were computed under this assumption.

In order to compute the fraction of the total neutral population in the $10G$ level from these measurements, it would be necessary to know the relative sensitivities of the Rydberg detector and the secondary emission neutral beam detector. Neither would it be easy to determine absolutely. Fortunately, the ratio of these sensitivities can be determined directly by comparing the strength of the $10G$ RESIS signal, observed as an increase in the Rydberg detector signal, and observed as a decrease in the neutral beam current. These two signals, denoted $S_{\text{Ryd det}}$ and S_{Neutral} should correspond to the same number of atoms,

$$\Delta N = T_{\text{ex}} N_{10G}, \tag{2}$$

the number excited from $10G$ to $30H$. In this expression, T_{ex} represents the excitation probability from $10G$ to $30H$, N_{10G} is the total number of atoms present in the $10G$ level, and ΔN is the change in either the total neutral beam flux or the ionizable Rydberg atom flux produced by the CO_2 laser. The ratio of these two signals corresponds to the ratio of sensitivities of the two detectors, including all efficiency factors such as collection and ionization efficiency. This sensitivity ratio was measured several times on several different days, using several different $n=10$ RESIS signals and targets, and always with consistent results. The final result was

$$\frac{S_{\text{Ryd det}}}{S_{\text{Neutral}}} = 1223(54) \equiv \kappa. \tag{3}$$

The statistical errors in this measurement are relatively large due to the difficulty of measuring the small change in the neutral current (about 0.5% for the $10G$ signal).

Using this ratio of sensitivities, each measured ratio of $10G$ RESIS signal to neutral beam could be converted into a fractional signal in the neutral beam channel:

$$\frac{S^{10G}_{\text{Neutral}}}{S^{\text{RT}}_{\text{Neutral}}} = \frac{1}{\kappa}\frac{S^{10G}_{\text{Ryd det}}}{S^{\text{RT}}_{\text{Neutral}}}. \tag{4}$$

The only other information required to compute the fractional population of the $10G$ level is the excitation efficiency, T_{ex}, of the CO_2 laser.

$$f_{10G} = \frac{N_{10G}}{N_{\text{Total}}} = \frac{2S^{10G}_{\text{Neutral}}}{T_{\text{ex}} S^{\text{RT}}_{\text{Neutral}}}. \tag{5}$$

In this expression, the factor of 2 occurs since the time-averaged RESIS signal is reduced by a factor of two by the 50% modulation of the Rydberg target. The only critical assumption underlying Eq. (5) is that *all* atoms excited by the CO_2 laser are lost from the neutral beam.

Because of the importance of T_{ex} in establishing the absolute population fractions, a careful study of the $10G$ excitation line shape and power saturation was carried out after the other measurements were completed. In the course of this study, it was determined that the previous data collection had been carried out with imperfect cancellation of the Earth's magnetic field, leading to a motional electric field of about 20 mV/cm at the interaction point between the CO_2 laser and the atomic beam. Figure 3(a) shows the amplitude of the $10G$-$30H$ RESIS signal as a function of laser power in the presence of this electric field. The smooth curve is a fit to

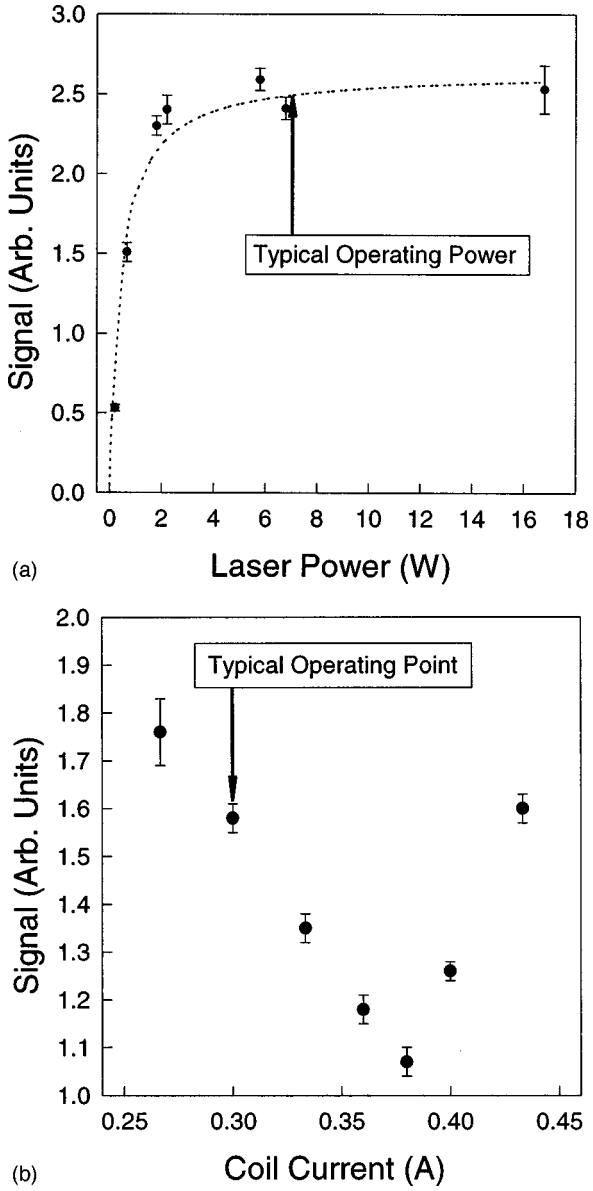

FIG. 3. (a) Saturation curve showing the amplitude of the $10G$-$30H$ RESIS signal as a function of the CO_2 laser power. The dashed line shows a fit described in the text. At the typical operating power, indicated by an arrow, the signal is well above saturation. (b) Amplitude of the $10G$-$30H$ RESIS signal as a function of the setting of the magnetic field coil used to compensate for the 500-mG field of the Earth. The net field is nearly zero at a coil setting of 0.38 A, where the RESIS signal has minimum amplitude. At the coil setting of 0.30 A, where signal measurements were made, a residual field of about 100 mG produces a motional electric field of about 20 mV/cm, which Stark broadens the RESIS resonances and increases the excitation probability to a value above 50%.

$$S(P) = \frac{S_{\text{max}}}{1 + P_{\text{sat}}/P}, \tag{6}$$

which is the form predicted by a simple 2-level rate equation model. The fit is satisfactory and indicates that the signal is

well above saturation at the operating powers of 5–7 W. This implies that all m values of the $10G$ level, for which the saturation power may vary by as much as a factor of two, will be excited with equal probability by the laser, and that the RESIS signal amplitude is a measure of the total population in all $10G$ levels.

The saturated excitation probability would not normally exceed 50% in a two-level system, but in our case, the presence of the 20 mV/cm motional field mixes the $30H$ level into the $n=30$ Stark manifold. At this field, the width of the Stark manifold is about 70 MHz, about twice the homogeneous linewidth, indicating that as many as 15 different Stark levels may be excited by the laser, and if they become dephased during the 180-ns transit time of the atom through the laser, they may act as a reservoir level that allows the total excitation probability to exceed 50%. Indeed, when the amplitude of this signal was measured as a function of the Helmholtz coil field that compensates for the Earth's magnetic field, the result of Fig. 3(b) was found. There is a clear minimum signal size at a coil setting of 0.38 A, somewhat larger than the 0.30 A used for collection of data, and corresponding closely with a net magnetic field of zero at the laser interaction point. Measurements of the RESIS signal at this point showed a linewidth of about 50 MHz, noticeably narrowed by the absence of Stark broadening. This linewidth could be accounted for by the known sources of inhomogeneous width, the angular distribution in the atomic beam (22 MHz), and the spin structure of the $10G$ level (25 MHz), which combine to give a total inhomogeneous width of 33 MHz, and a power broadened homogeneous width of 35 MHz. The homogeneous width and rate of power broadening agreed with theoretical simulations which included the Gaussian profile of the beam and a 50 ns phase relaxation time. Measurements of the signal amplitude as a function of laser power, in the absence of Stark broadening, showed that the signal was still well saturated at the operating powers, in agreement with the simulations. Since the signal is saturated here and the inhomogeneous width is less than the homogeneous width, we will assume that the excitation probability at the minimum of Fig. 3(b) is 50(10)%. This implies that at the coil setting used for data collection (0.90), the excitation probability was 1.5 times larger,

$$T_{\mathrm{ex}}=0.75(15). \tag{7}$$

The uncertainty in T_{ex} is the limiting factor in the precision of determinations of the absolute population fractions in this experiment.

Using Eqs. (4) and (5), the measured S/I ratios can be converted, for each choice of target, to the fractional population of the $10G$ level at the laser interaction point. These results are shown in Table I. The $10G$ population fraction at the time of capture is about a factor of 3 larger than the fraction measured at the CO_2 laser interaction due to the spontaneous decay of the $10G$ level in the intervening 1.9 μs ($\tau_{10G}=1.81$ μs). More generally, both cascades from higher populated levels and radiative transitions stimulated by blackbody radiation could also alter the populations during this time period. A numerical simulation, based on the excited state population distributions predicted by CTMC calculations, and including both spontaneous and stimulated transitions in a 300-K radiation field indicated that the conversion between populations at the CO_2 laser and at the Rydberg target is modified by 5 to 40% beyond the simple effects of spontaneous decay of the nL level. Specifically, these simulations showed that

$$N_{nL}(1.9\ \ \mu\mathrm{s})=N_{nL}(0)e^{-1.9\ \ \mu\mathrm{s}/\tau_{nL}}F_{nL}, \tag{8}$$

where τ_{nL} are the spontaneous lifetimes of each level [9] and F_{nL} are the correction factors are shown in Table I. Also shown in Table I are the final results deduced for the fractional $10G$, $10H$, and 10 high-L ($L=7,8,9$) populations produced in the Rydberg target, for each value of n_t. The error bars shown on the experimental measurements represent only the statistical errors, and do not include the 20% error in the vertical scale arising (largely) from the estimate of $10G$ excitation efficiency. Population fractions for the $9G$ level, obtained from exciting the $9G$-$20H$ transition are also shown. Their absolute value is probably underestimated since they were obtained from the observed S/I measurements by assuming the same value of the constant κ, from Eq. (2). The ionization and collection efficiency of the $n=20$ levels is expected to be lower than the $n=30$ levels, by perhaps a factor of 3 [10], but, unfortunately, no independent measurement of the constant κ was made for the $9G$ signals. In the absence of better information, we assume the value of T_{ex} measured for the $n=10$ signals applies to the $9G$ signal as well.

All the measurements of Table I were obtained with the post-target electric field region set to 3300 V/cm. These ionized electrons were captured to higher n levels, reducing the detector background and increasing the signal-to-noise ratio for the RESIS signals. Since the entry and exit times for this field were about 50 ns, it is expected that the $n=9$ and 10 levels, especially the G and H levels, will pass adiabatically through the 100-ns field, leaving their populations virtually unchanged. Comparison of the $10G$ and $10H$ RESIS signals with the 3300-V/cm field and with a much smaller field (20 V/cm), which was just sufficient to deflect residual ions from the beam, showed very little difference in the signal sizes. These tests showed that the signals were, on the average, about 5% larger with the 3300-V/cm field. Since the presence of the strong field should increase the signals slightly by ionizing the upper levels of the RESIS transitions, these measurements were taken as confirmation that the $n=10$ level populations were largely unchanged by the field. With the strong field present, as during the measurements, these upper levels could be regarded as empty prior to the CO_2 laser.

The final column of Table I shows the CTMC predictions for the fractional population of the $10G$ level at capture. These predictions were obtained assuming that the target obtained by exciting the nF level is a 50/50 mixture of nF and $(n+1)D$ levels. This is the expected distribution of target populations when the excitation is well above the threshold for population sharing by maser action, as it was for all targets. The CTMC calculations were carried out separately for all nF and nD targets, using an approach described previously [11–13]. Hamilton's equations of motion for a fully three-dimensional three-body problem were solved numerically. The forces between all three bodies, the projectile ion,

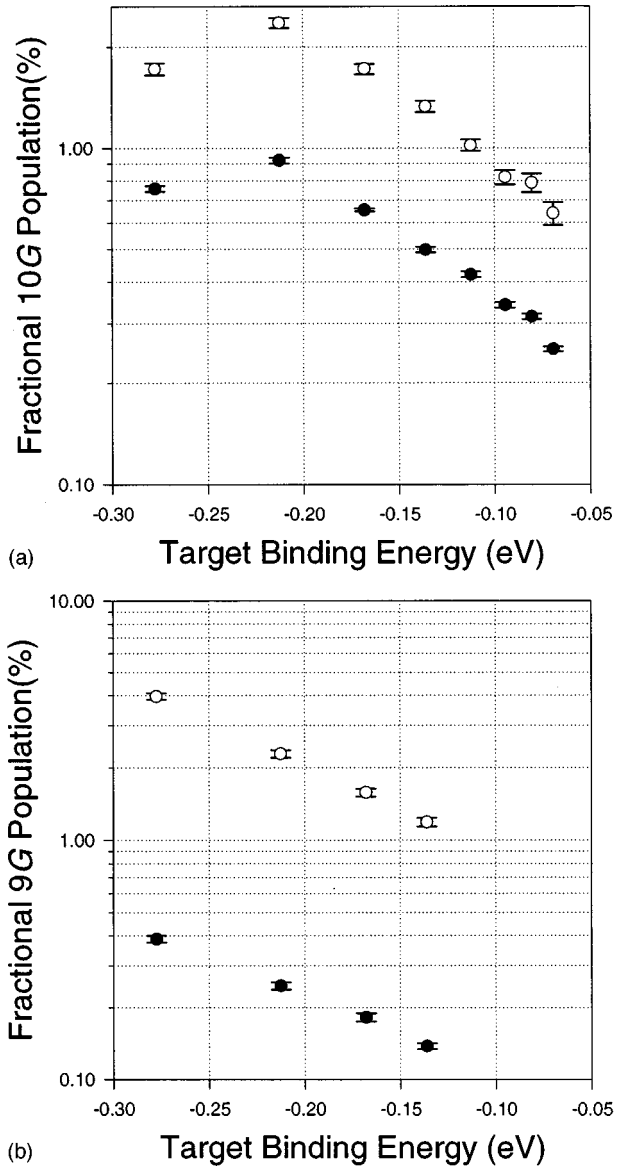

FIG. 4. (a) Population fractions of the helium $10G$ level (N_{10G}/N_{Total}) as a function of the binding energy of the Rb Rydberg target. The measured population fractions (solid points) show a peak fraction of about 1% for the $8F$ target. The dependence of the population fraction on target binding energy closely matches the predictions of CTMC calculations (open points), but the measured fractions are uniformly smaller than theory by a factor of about 2.5. Experimental error bars are statistical only, and do not include a common systematic error of 20%. (b) Population fractions of the helium $9G$ level for a few of the Rydberg targets. The absolute value of these fractions is uncertain by about a factor of 3. The relative fractions show good agreement with the theory for the dependence on target binding energy. In particular, the target energy that maximizes the population fraction shows the expected downward shift, relative to the $10G$ measurements.

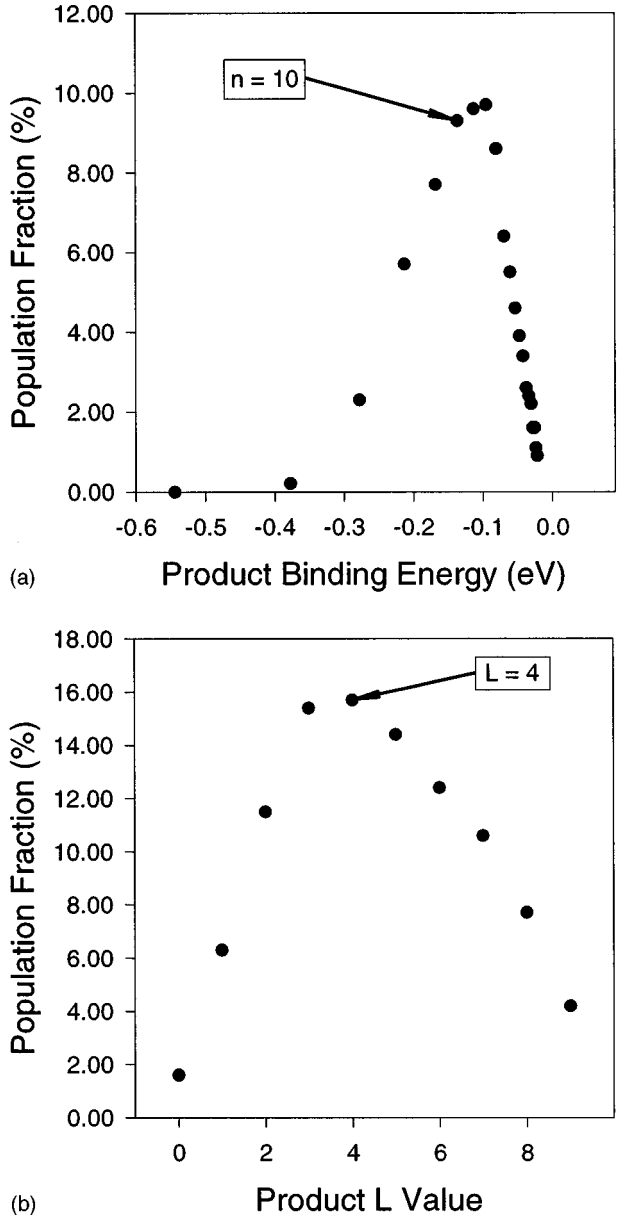

FIG. 5. Population distributions predicted with CTMC for capture at $v=0.1$ a.u. on the $10F/11D$ Rydberg target. (a) n distribution and (b) L distribution within $n=10$. Note the $10G$ level is near the maximum of both distributions.

the target nucleus, and the target electron, were taken to be Coulombic, and were fully included. The target electron is described by a microcanonical ensemble of classical Kepler orbits corresponding to the correct total energy of the target (E_t), and (as described below) the target angular momentum (L_t). This is implemented by choosing the initial conditions based on six random numbers, the projectile impact parameter, the electron's orbital phase, the three Euler angles defining the orientation of the electron orbit relative to the projectile axis, and the orbital eccentricity, which is constrained to lie in an interval determined by the target electron's angular momentum. For each set of initial conditions, the classical equations of motion determine the eventual outcome, and if the electron is found to undergo charge capture, its final quantum numbers are assigned based on its final orbit. The capture cross section is determined from the ratio of trajectories undergoing capture to the total number calculated. For this study, a total of 100 000 trajectories were calculated for each of the 16 targets.

The comparison between measured and predicted $10G$ population fractions is shown graphically in Fig. 4(a). The horizontal scale is the binding energy of the various Rydberg targets, in eV. The measured and predicted population frac-

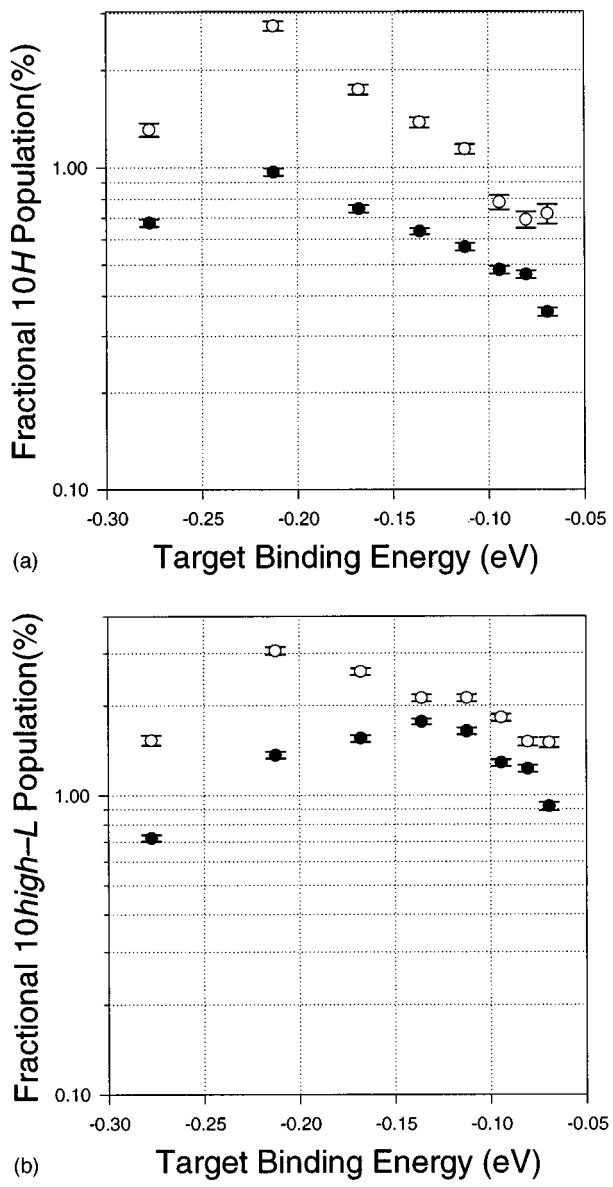

FIG. 6. Measured and calculated population fractions for (a) helium 10H level and (b) helium 10 high-L ($L=7,8,9$) levels. Measured fractions (solid points) and theoretical predictions (open points) are shown as in Fig. 4.

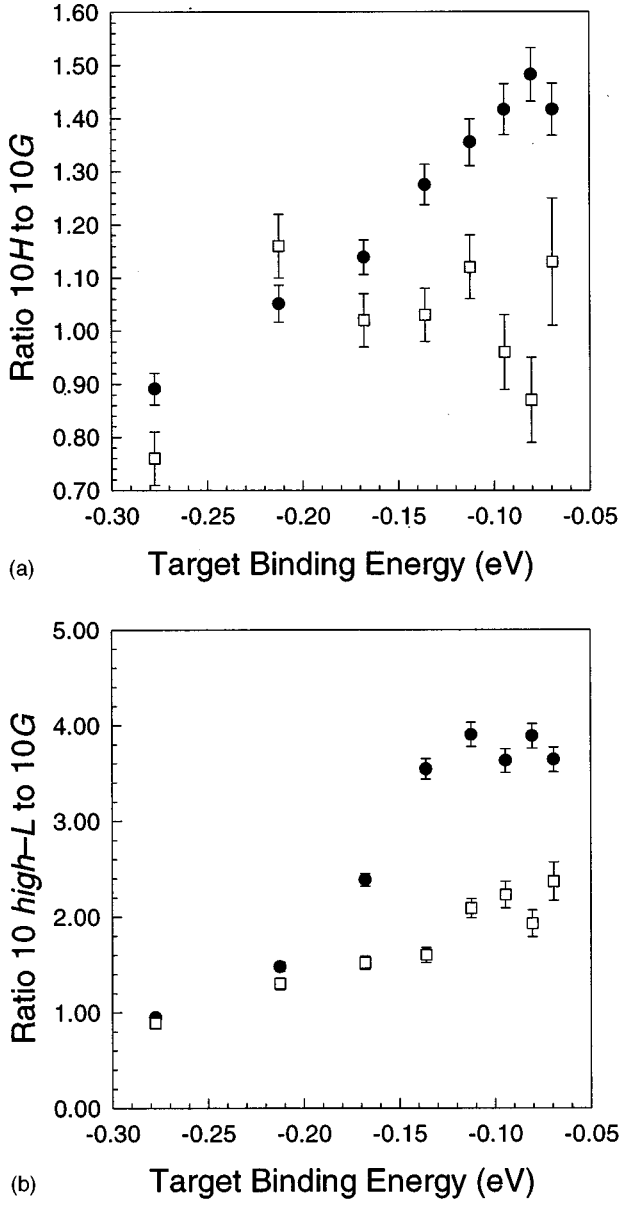

FIG. 7. Ratios of population fractions measured for $n=10$ helium levels of different L, plotted vs the Rydberg target binding energy. (a) Ratio of 10H to 10G population fractions. (b) Ratio of 10 high-L to 10G population fractions. In both cases, the measured ratios are shown as solid points, while the predictions of CTMC calculations are shown as open points. These theoretical predictions have rather large statistical errors.

tions for the 10G level show very good agreement for the dependence on E_t, but disagree on the magnitude of the population fraction by about a factor of 2.5. The good agreement versus E_t confirms one aspect of the energy-resonant capture process, but the disagreement over the absolute value of the capture fraction suggests that a wider distribution of final n or L levels is produced in the capture than predicted by the theory. Figure 5 illustrates the population distributions, in n and L, predicted by the CTMC code for capture from the 10F/11D target. It can be seen that the 10G level is near the maximum of both distributions. If either or both distributions were significantly broader in nature, than in the CTMC prediction, this could account for the factor of 2.5 discrepancy in the absolute capture fraction.

A similar comparison for the 9G population fractions is shown in Fig. 4(b), over a more limited range of n_t. Again, the dependence on E_t is very well reproduced. This is significant because it shows the expected downward shift in the position of the maximum population fraction in n_t, as compared with the 10G measurements. Since, as discussed above, the 9G fraction is probably underestimated by the use of the calibration constant κ measured for the $n=10$ signals, the factor of 7 discrepancy between measured and calculated 9G population fractions should not be taken too seriously. Instead, the 9G population fraction is best regarded as a relative measurement, with the absolute scale undetermined.

Similar measurements were made for the 10H level and for the 10 high-L ($L=7,8,9$) peak of Fig. 2. These were converted into fractional populations at capture in the same manner as the 10G measurements, and are also shown in

Table I along with the corresponding predictions from CTMC. Comparisons between these results and the CTMC predictions are shown in Fig. 6. The 10*H* comparison, Fig. 6(a), appears similar to that for 10*G*, except that the experimental result rises somewhat, relative to the theory at higher n_t. The *high-L* results, Fig. 6(b), show a rather dramatic difference. For the lower n_t targets, the *high-L* population fraction is below theory by about a factor similar to the 10*G* and 10*H*. The higher n_t targets, by contrast, show a much larger *high-L* population fraction, close to the level predicted by theory. One way to illustrate the differences between 10*G*, *H*, and *high-L* population fractions is to plot their ratios. This has the additional advantage of being independent of the uncertainties in the absolute capture fractions. Such a comparison is shown in Fig. 7, where the ratios of 10*H* to 10*G* population fractions, and of 10 *high-L* to 10*G* population fractions are shown. Both experimental ratios show a smooth trend favoring the higher *L* levels as n_t increases. In the case of the *high-L* to *G* ratio, the ratio changes by a factor of 4 over this range of targets. Neither of these trends appears to be predicted by the CTMC simulations, shown by open points in Fig. 7.

To summarize, we have used the RESIS technique to study collisions between He^+ ions at 0.1-a.u. velocity and Rb Rydberg targets with $7 \leqslant nt \leqslant 14$. The measurements determine, with unprecedented detail, certain facts about the reaction that can be used to test the accuracy of present and future theoretical models. At present, the only theoretical model known to us that can provide detailed predictions of this reaction is CTMC, and we have therefore tested its predictions against the measurements reported here. On the whole, we find very reasonable agreement. In particular, the dependence of f_{10G} and f_{9G} on n_t predicted by CTMC is in close agreement with our measurements. This is significant since it suggests that the classical CTMC contains all the essential physics related to the energy ''resonance'' that occurs in the charge transfer. (A more definitive conclusion should probably await measurements under a wider range of conditions.) In spite of this, we know of no simple classical argument that can predict the width of this energy resonance, except by noting the results of repeated CTMC calculations. On the other hand, other aspects of our measurements are poorly predicted by CTMC, including the absolute value of f_{10G} and the magnitude of the tendency to favor higher-*L* levels as n_t increases. These discrepancies may provide clues to the as yet unknown limits of validity of CTMC and yardsticks against which improved theories can be measured.

Unlike previous studies of final-state distributions after resonant charge transfer, the RESIS method used here does not rely on field ionization for discrimination of the final states. Instead, the highly selective postcollision laser excitation is used to determine population fractions in particular final n,L levels. The scatter in the measured values is quite small, and consequently the uncertainties in the relative population fractions are quite small. The dominant source of uncertainty in the absolute population fractions reported here is the estimate of the laser excitation probability. In the future, it may be possible to reduce this uncertainty by more extensive studies, which, for example, involve more than one laser excitation region, but it is likely to remain the precision limiting factor in this technique. Even so, the RESIS method of studying final-state distributions in resonant charge-transfer collisions should make possible a wide range of unambiguous and quantitative characterizations of charge-transfer collisions.

ACKNOWLEDGMENTS

This work was supported by the Division of Chemical Sciences, Office of Basic Energy Sciences, Office of Basic Energy Research, U.S. Department of Energy.

[1] J. Pascale, R. E. Olson, and C. O. Reinhold, Phys. Rev. A **42**, 5305 (1990).
[2] K. B. MacAdam, L. G. Gray, and R. G. Rolfes, Phys. Rev. A **42**, 5269 (1990).
[3] Thomas F. Gallagher, *Rydberg Atoms* (Cambridge Univ. Press, Cambridge, England, 1994).
[4] A. Pesnelle *et al.*, Phys. Rev. Lett. **74**, 4169 (1995).
[5] A. Pesnelle *et al.*, Phys. Rev. A **54**, 4051 (1996).
[6] F. J. Deck, E. A. Hessels, and S. R. Lundeen, Phys. Rev. A **48**, 4400 (1993).
[7] F. J. Deck, Ph.D. thesis, Univ. of Notre Dame (1993).
[8] C. W. Fehrenbach, S. R. Lundeen, and O. L. Weaver, Phys. Rev. A **51**, R910 (1995).
[9] Radiative lifetimes for the levels under study were taken to be 9*G*: 1.322 μs, 10*G*: 1.814 μs, 10*H*: 2.747 μs, 10 K: 5.211 μs, 10*L*: 6.722 μs, 10*M*: 8.423 μs.
[10] Ionization of the $n=20$ level in the Rydberg detector required a substantially larger field. This was obtained with a potential of 9000 V across a gap of 8 mm. Inhomogeneities in this ionization field resulting from the 6-mm-diameter apertures prevented the RESIS ions from being focused as tightly as in the $n=30$ case.
[11] R. E. Olson and A. Salop, Phys. Rev. A **16**, 531 (1977).
[12] R. E. Olson, J. Phys. B **13**, 483 (1980).
[13] A. P. Hickman, R. E. Olson, and J. Pascale, in *Rydberg States of Atoms and Molecules*, edited by R. F. Stebbings and F. B. Dunning (Cambridge University Press, Cambridge, England, 1983).